

Decomposing the Energetic Impact of Drug Resistant Mutations in HIV-1 Protease on Binding DRV

Yufeng Cai and Celia A. Schiffer*

Department of Biochemistry and Molecular Pharmacology, University of Massachusetts Medical School, 364 Plantation Street, Worcester, Massachusetts 01605

Received September 4, 2009

Abstract: Darunavir (DRV) is a high affinity (4.5×10^{-12} M, $\Delta G = -15.2$ kcal/mol) HIV-1 protease inhibitor. Two drug-resistant protease variants FLAP+ (L10I, G48V, I54V, V82A) and ACT (V82T, I84V) decrease the binding affinity with DRV by 1.0 and 1.6 kcal/mol, respectively. In this study, the absolute and relative binding free energies of DRV with wild-type protease, FLAP+, and ACT were calculated with MM-PB/GBSA and thermodynamic integration methods, respectively. Free energy decomposition elucidated that the mutations conferred resistance by distorting the active site of HIV-1 protease so that the residues that lost binding free energy were not limited to the sites of mutation. Specifically the bis-tetrahydrofuranylurethane moiety of DRV maintained interactions with the FLAP+ and ACT variants, whereas the 4-amino phenyl group lost more binding free energy with the protease in the FLAP+ and ACT complexes than in the wild-type protease, which could account for the majority of the loss in binding free energy. This suggested that replacement of the 4-amino phenyl group might generate new inhibitors less susceptible to the drug resistant mutations.

1. Introduction

The human immunodeficiency virus type 1 (HIV-1, see Abbreviations section at the end for a summary of the abbreviations used in this work) protease is a homodimeric aspartyl enzyme with 99 residues in each chain. The two HIV-1 monomers are bound by nonbonded interactions, with the active site at the interface between the two monomers.¹ The protease processes the viral Gag-Pol polyprotein, yielding the structural proteins and enzymes critical for the maturation of infectious viral particles.² Thus, HIV-1 protease has been a major target for structure-based drug design. Nine protease inhibitors have been approved by the Food and Drug Administration (FDA) for HIV therapy, effectively decreasing the mortality rate of HIV/AIDS patients.³ These FDA-approved HIV-1 protease inhibitors, developed at least in part using structure based drug design, are competitive inhibitors.² Unfortunately, exposure to protease inhibitors selects for viruses that have acquired drug resistance mutations in protease due to the high replication rate of HIV-1 and to lack of a proofreading mechanism in its reverse

transcriptase. These drug-resistant protease variants lose their high binding affinity to the inhibitors, while maintaining enough enzyme activity for the virus to propagate.⁴

To understand the basis for these changes in drug-resistant proteases, over 200 crystal structures of HIV-1 protease variants have been solved in the past 25 years. Changes in affinity due to drug resistant mutations and thus the thermodynamics of binding can be measured by isothermal titration calorimetry.^{5,6} Comparison between the structures of wild-type and drug-resistant variant proteases in complex with inhibitors partially elucidates how specific protease mutations decrease protease–inhibitor binding affinity.^{7,8} However, elucidating the critical components of the binding affinity quantitatively from the structural data still remains a challenge. Free-energy simulations,^{9–15} in principle, can aid in elucidating these components of the binding affinities to particular atomic interactions.

Among these computational methods, free-energy perturbation (FEP) and thermodynamic integration (TI) methods, which are derived from statistical mechanics,^{12,16–21} are mostly used with the thermodynamic cycle to calculate relative binding free energy changes in similar systems. The

* Corresponding author e-mail: celia.schiffer@umassmed.edu.

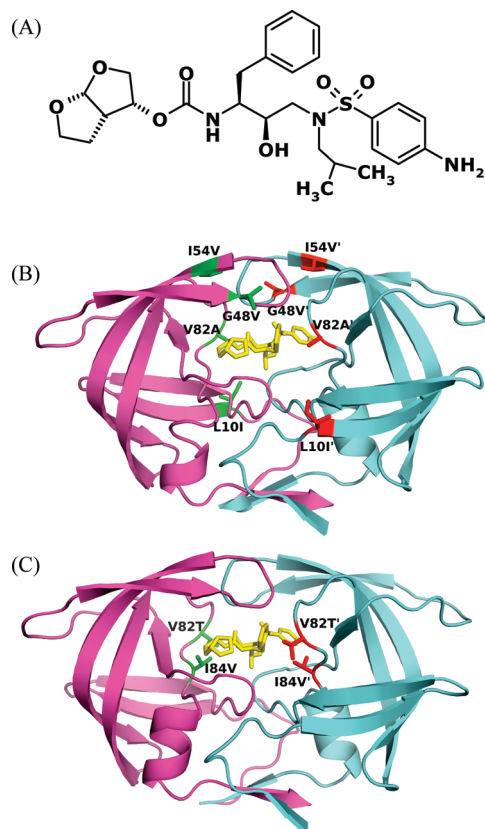


Figure 1. (A) Chemical structure of DRV. (B) Crystal structure of protease variant FLAP+-DRV complex 3EKT.⁶⁶ DRV is colored yellow. The side chains of the mutated residues Ile10, Val48, Val54, and Ala82 are displayed and colored red or green. (C) Structure of protease variant ACT-DRV complex 1T7I.⁵ DRV is colored yellow. The side chains of the mutated residues Thr82 and Val84 are displayed and colored red or green.

molecular-mechanics Poisson–Boltzmann surface area (MM-PBSA) method combines molecular mechanics and the continuum solvation model.^{13,22–26} Solvation properties can be described by the Poisson–Boltzmann (PB) or generalized Born (GB) equation. This method is reliable and applicable to calculating absolute binding free energy change associates with biomolecular recognitions. To achieve a better match with experimental data, the MM-PB/GBSA method is usually supplemented by rough entropy estimation. Free-energy calculation methods provide a way to estimate the binding free energy of inhibitors with different protease variants, allowing computational screening of lead compounds in rational drug design. Furthermore, the calculation results can be further analyzed, e.g., for free energy decomposition, to provide information about affinity changes due to specific kinds of interaction on an atomic level, which could not be determined by experimental methods.^{13,22,27,28}

The HIV-1 protease inhibitor, Darunavir (DRV, formerly known as TMC114; Figure 1A) has recently been approved by the FDA.²⁹ This second-generation protease inhibitor, which was developed after extensive effort in rational drug design,³⁰ binds the most tightly to the protease of all known inhibitors ($K_d = 4.5 \times 10^{-12}$ M).⁵ Nonetheless, DRV still loses affinity to drug resistant variants of HIV-1 protease.⁵ In this study, the binding of DRV was investigated with wild-

type HIV-1 protease and two drug-resistant variants: FLAP+ (Figure 1B) with L10I, G48V, I54V, and V82A, which are a combination of flap and active site mutations, and ACT (Figure 1C) with V82T and I84V, which are active site mutations. Each of these three systems was analyzed in three parallel 20 ns molecular dynamics (MD) simulations using initial coordinates from their crystal structures. In these MD simulation trajectories, the MM-PBSA and MM-GBSA methods were applied to calculate changes in binding free energy, which were compared with ITC results. The classical TI method was also used to calculate and compare differences in binding free energy of the DRV-ACT and DRV-WT complexes. The accuracy, convergence, and reproducibility of the calculated results have been compared and discussed. The MM-PB/GBSA correctly predicted the order of binding affinity of DRV-WT, DRV-Flap+, and DRV-ACT. The TI calculation result is in good agreement with the experimental data. Free energy component analysis is performed to elucidate the mechanism for resistance of FLAP+ and ACT to DRV. The free energy decomposition study results show that the bis-THF group of DRV has maintained its favorable van der Waals (vdW) contact with the protease even in the drug resistant variants. Understanding how the protease mutates to decrease its binding affinity with a very high affinity inhibitor will contribute to developing better strategies to design protease inhibitors.

2. Methods

2.1. MD Simulation with the Program Sander in the AMBER 8 Package. The initial coordinates of the DRV-WT, DRV-FLAP+, and DRV-ACT protease complexes were taken from each of their respective cocrystal structures 1T3R,⁵ 3EKT, and 1T7I.⁵

Molecular dynamics simulations were performed using the program Sander in the MD simulation package AMBER 8.³¹ For the standard protease residues, the atomic partial charges, van der Waals parameters, equilibrium bond lengths, bond angles, dihedral angles, and their relative force constants were taken from the AMBER database (ff03).³² For DRV parameters, the van der Waals parameters, equilibrium bond lengths, bond angles, dihedral angles, and force constants were taken from the General AMBER Force Field database.³³ The partial charges of inhibitor atoms were obtained as follows. First, the coordinates of the DRV atoms were taken from the 1T3R crystal structure and the missing hydrogen atoms added by the program Quanta. Second, the geometry of the resulting structure was optimized with the (HF)/6-31G* basis set by the Gaussian 03 package.³⁴ Finally, the resulting electrostatic potential was used in the RESP³⁵ module of the AMBER 8 package to derive the atomic partial charges of the inhibitor.

The explicit solvent model was applied to all systems. Each structure was solvated with the TIP3P water cubic box to allow for at least 8 Å of solvent on each face of the protease. The vdW dimensions for the protease were 44 by 35 by 59 Å. The dimensions of the final periodic box were 63 by 55 by 78 Å. The simulation system had approximately

7000 water molecules, and six Cl^- counterions were added to balance the charge of the system.

A three-step energy minimization process with the steepest descent method was used to allow the system to reach an energetically favorable conformation. In the first energy minimization step, all the heavy atoms of the protease were restrained with a harmonic force constant of 10 kcal mol⁻¹ Å⁻². In the second step, only the backbone nitrogen, oxygen, and carbon atoms were restrained. The strength of the restraint was maintained as 10 kcal mol⁻¹ Å⁻². In the third step, the restraint was turned off, and all atoms were allowed to move. Each of the three steps had 2000 cycles. The temperature of the energy-minimized system was then gradually raised from 50 K to 300 K in the NVT ensemble. Initial velocities were assigned according to the Maxwellian distribution, and random seeds were assigned with three different values to generate nine simulations, three parallel simulations for each of the WT-DRV, FLAP+-DRV, and ACT-DRV systems. In the thermalization process, heavy atoms were restrained with a harmonic force constant of 10 kcal mol⁻¹ Å⁻². The whole process was 50 ps (50 000 steps, each of which was 1 fs). A 50 ps equilibration was then performed in the NPT ensemble without restraining heavy atoms. In the subsequent sampling MD simulations, each step was 2 fs, and the total simulation was 20 ns. For the thermalization, equilibration, and sampling simulations, the SHAKE algorithm³⁶ was applied to constrain all hydrogen atoms.

2.2. MM-PB/GBSA Method. For the protease-ligand system, the binding free energy change is represented by



and

$$\Delta G_{\text{binding}} = \Delta G_{\text{MM}} - T\Delta S + \Delta G_{\text{PB/GB}} + \Delta G_{\text{NP}}$$

where

$$\Delta G_{\text{MM}} = \Delta G_{\text{bond}} + \Delta G_{\text{angle}} + \Delta G_{\text{dih}} + \Delta G_{\text{vdW}} + \Delta G_{\text{ele}}$$

$$\Delta S = \Delta S_{\text{translational}} + \Delta S_{\text{rotational}} + \Delta S_{\text{vibrational}}$$

The molecular mechanical energy ΔG_{MM} is the estimated free energy change associated with the binding process in the gas phase. ΔG_{MM} was calculated by standard force field functions and parameters. Depending on the type of interaction, ΔG_{MM} has two kinds of energetic terms: bonded and nonbonded. The bonded term includes terms representing bond stretching energy (ΔG_{bond}), angle vibrational energy (ΔG_{angle}), and dihedral angle torsion energy ($\Delta G_{\text{dihedral}}$). The nonbonded term includes terms representing the van der Waals interaction energy (ΔG_{vdW}) and electrostatic interaction energy (ΔG_{ele}).

The polar component of the solvation free energy, represented by $\Delta G_{\text{PB/GB}}$, can be calculated either by solving the Poisson-Boltzmann equation (PB method) or the generalized Born equation (GB method). The nonpolar component of the solvation free energy is represented by ΔG_{NP} . The sum of $\Delta G_{\text{PB/GB}}$ and ΔG_{NP} estimates the free

energy change associated with molecules entering solvation from the gas phase. The GB calculation was done using the model developed by Onufriev et al.^{37,38} The PB calculation was done with the AMBER 8 numerical PB solver.³⁹ The solute dielectric constant is 1.0, and the solvent dielectric constant is 80.0. ΔG_{NP} was calculated by the LCPO (linear combinations of pairwise overlaps) method, which is linearly dependent on the solvent access surface area: $\Delta G_{\text{NP}} = 0.0072 \times \text{SASA}$.⁴⁰ The entropy was calculated by normal-mode analysis using the AMBER 8 NMODE module.^{26,41} For every 20 ps of the 20 ns MD simulation trajectory, a snapshot of the protease and inhibitor was taken removing the solvent and counterions. The total number of the atoms for each of the three systems DRV-WT, DRV-FLAP+, and DRV-ACT were 3203, 3209, and 3203, respectively. Altogether, 1000 frames were used for the MM-PB/GBSA calculations. The time-consuming entropy calculations were performed on 100 frames.

2.3. Thermodynamic Integration Method. When studying drug-resistant protease mutants, the binding free energy relative to wild-type protease is even more important than the absolute binding free energy. The thermodynamic integration method^{42,43} was applied to the protease-inhibitor system to compute the free-energy difference between different states of the system. From statistical mechanics, the Gibbs free energy (G) can be calculated from the partition function Q as follows:

$$G = -RT \ln Q \quad (1)$$

The partition function can be expressed as the integral of the system's Hamiltonian function $H(r,p)$. After a coupling parameter, λ , is introduced into the Hamiltonian, Q can be expressed as

$$Q = \int \int dr dp \exp(-H(r,p,\lambda)/RT) \quad (2)$$

From eqs 1 and 2, the derivative of G with respect to λ is

$$\frac{dG}{d\lambda} = \frac{\int \int \frac{dH(r,p,\lambda)}{d\lambda} e^{-H(r,p,\lambda)/RT} dr dp}{\int \int e^{-H(r,p,\lambda)/RT} dr dp} = \left\langle \frac{dH(r,p,\lambda)}{d\lambda} \right\rangle_\lambda \quad (3)$$

and

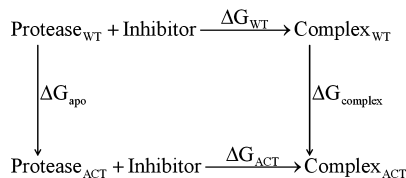
$$\Delta G = \int_0^1 \left\langle \frac{\partial H(\lambda)}{\partial \lambda} \right\rangle_\lambda d\lambda \quad (4)$$

Equation 4 is the master equation of the thermodynamic integration method. When applying this equation to the protein-ligand system, the kinetic component of the Hamiltonian can be neglected. Thus, the λ -coupling force field function $V(\lambda,r)$ was used to replace the Hamiltonian. The λ was chosen such that, when it equals zero, the force field function $V(0)$ and its relative parameters were correlated with the wild-type protease. When $\lambda = 1$, $V(1)$ and its parameters were correlated with the mutant protease. The numerical estimation of eq 4 was

$$\Delta G \approx \sum_{i=1}^n w_i \left(\frac{\partial V}{\partial \lambda} \right)_{\lambda i} \quad (5)$$

The λ values and their relative weights (Table 5) were assigned from the Gaussian quadratic formula.

Directly calculating thermodynamic integration from the unbound to the bound state is not feasible. The thermodynamic cycle below was used since G represents a state function and is independent of the path.



As shown above, instead of calculating the free energy changes ΔG_{WT} and ΔG_{ACT} associated with the chemical reaction path, the ΔG_{apo} and $\Delta G_{complex}$ through the “alchemical” path^{44–46} were calculated.

Thus, the drug-resistant mutant’s loss of binding free energy compared to the wild-type protease was represented by

$$\Delta \Delta G = \Delta G_{ACT} - \Delta G_{WT} = \Delta G_{complex} - \Delta G_{apo} \quad (6)$$

The thermodynamic integrations were carried out in the Sander module of the AMBER 8 package.^{47,48} The wild-type and mutant proteases have different numbers of side chain atoms on the mutated residues. To keep the same number of atoms in the initial and final states, we perturbed the extra atoms to dummy atoms, which had no nonbonding interactions with the rest of the system. For the ACT mutant, both mutated residues (V82T and I84V) have fewer atoms than the wild type. Thus, the perturbation was done from WT to ACT (Figure 2).

The DRV–WT crystal structure 1T3R was used to generate the coordinates file for the calculation of the $\Delta G_{complex}$. For the calculation of ΔG_{apo} , two sets of coordinates were used. One was from the unbound wildtype protease crystal structure 1HHP. The other one was the protease atoms coordinates from the WT–DRV complex crystal structure 1T3R with the inhibitor of DRV deleted from the set of coordinates. The three-step energy minimization was performed as described above. The structure was then thermalized and pre-equilibrated with a harmonic restrained force, and the λ value was 0.5. During the thermalization, different random seed values were assigned to create parallel calculations as controls. The pre-equilibrated structure was then sampled at 12 λ values, see Table S1 (Supporting Information). The pre-equilibrated structure was then used to start the 12 independent simulations with different corresponding λ values (Table S1). The time steps were 1 fs, and the time for the calculation at each λ value was 2 ns. Thus, the total sampling time for each alchemical free energy change calculation was 24 ns. The expected error in the free energy calculations was the root-mean-square deviation in the energies of the sample in production period divided by the square root of the number of independent samples in the production period.⁴⁹

$$\text{expected error} = \frac{\text{sample rms}}{\sqrt{\text{number of independent samples}}} \quad (7)$$

3. Results

3.1. Comparison between Predicted Binding Affinity and ITC Data. *3.1.1. Calculations of Absolute Binding Free Energy by MM-PBSA and MM-GBSA Methods.* To evaluate the reproducibility and convergence of our free-energy calculation results, the same MM-GBSA protocol was applied to three independent 20 ns MD simulation runs of each of the WT–DRV, FLAP+–DRV, and ACT–DRV systems starting from each of their corresponding crystal structure (see the Methods section). To study the structural stability of the systems, the root-mean-square displacements (rmsd) of the C α atoms of the simulated proteins were plotted over time with respect to their corresponding crystal structures (Supporting Information, Figure S2). For all the DRV–protease systems after 2 ns of MD simulations, the rmsd values were approximately 1.5 Å. As the calculations all require extensive equilibration, the averages of potential production periods were evaluated. After 10 ns simulations, the calculated binding free energy for DRV–WT stabilized (Figure 3A) for all three parallel simulations. Each of the triplicates of DRV–FLAP+ and DRV–ACT stabilized within 6 and 9 ns, respectively (Supporting Information, Figure S1). Thus, the first 10 ns was used as the equilibration period, as the free energy did not converge between the runs

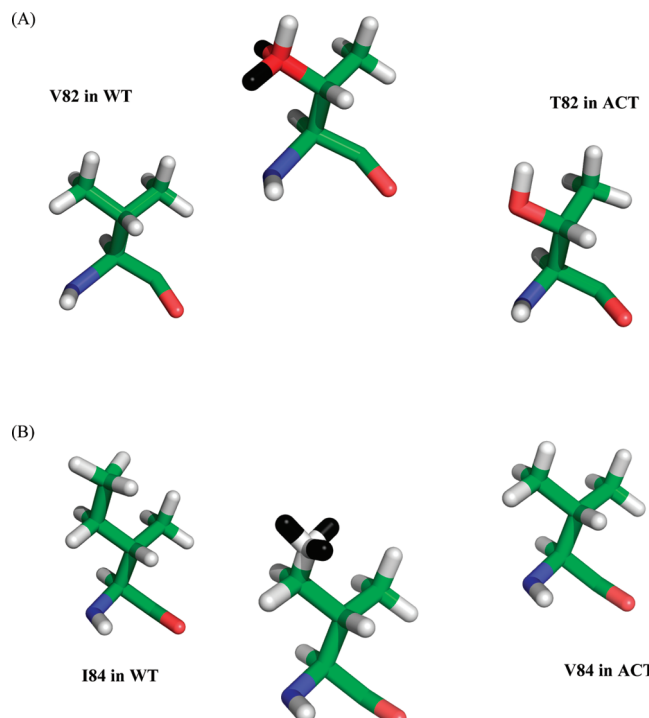


Figure 2. Perturbation of Val82 to Thr and Ile84 to Val. Hydrogen atoms are colored white, oxygen atoms are colored red, nitrogen atoms are colored blue, carbon atoms are colored green, and dummy atoms are colored black. Left: residue in the wild-type protease as the initial state. Middle: the hybrid residue in the calculation process. Right: the mutated residue as end state. (A) The perturbation of Val82 to Thr82. (B) The perturbation of Ile84 to Val84.

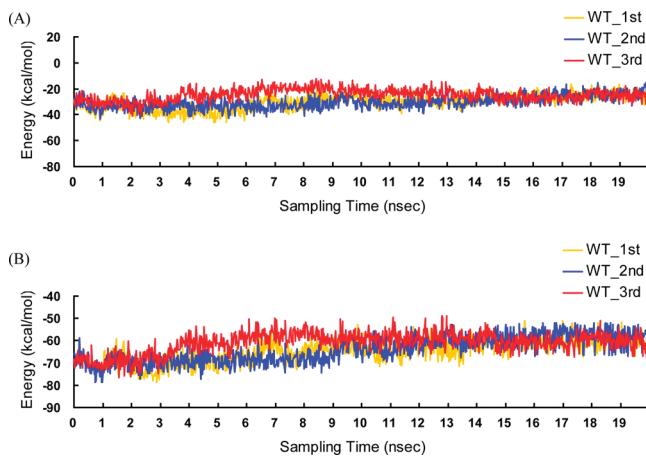


Figure 3. (A) MM-GBSA calculated results of DRV–protease binding free energy with respect to the time. The three curves represent three independent MD trajectories. (B) vdW energy component of DRV–WT binding free energy with respect to the time.

Table 1. Results of MM-GBSA Calculation for Absolute Binding Free Energy (kcal/mol) of DRV–Protease Based on Equilibration (1–10 ns) and Production (11–20 ns) Periods

protease	sampling time (ns)	run 1	run 2	run 3	average
WT	1–10	-33.4	-32.8	-24.9	-30.4
	11–20	-27.3	-27.0	-25.7	-26.7
Flap+	1–10	-23.4	-17.7	-20.1	-20.4
	11–20	-21.1	-20.8	-21.1	-21.0
ACT	1–10	-20.3	-13.9	-25.5	-19.9
	11–20	-17.8	-17.6	-19.8	-18.4

(Table 1), while the second 10 ns was used as the production period, since generally the runs were converged.

The average predicted binding free energy of WT–DRV was -26.7 kcal/mol, that of FLAP+–DRV was -21.0 kcal/mol, and that of ACT–DRV was -18.4 kcal/mol (Table 2). Although these values differed from the ITC experimental values for each system (-15.2 kcal/mol for WT–DRV, -14.2 kcal/mol for FLAP+–DRV, and -13.6 kcal/mol for ACT–DRV), they correctly ranked the three protease variants' binding free energies: WT > FLAP+ > ACT. The more rigorous and time-consuming PB method was also used to calculate the polar solvation free energy. With this method, the predicted results were in better agreement with the ITC experimental data: -15.1 kcal/mol for WT–DRV, -11.6 kcal/mol for FLAP+–DRV, and -10.5 kcal/mol for ACT–DRV (Table 2). Comparison of the predicted polar solvation free energy difference calculated using the GB and PB models showed that the GB model had underestimated the polar solvation free energy of all three systems. This difference in estimates of polar solvation free energy by the GB and PB models has been reported and discussed in

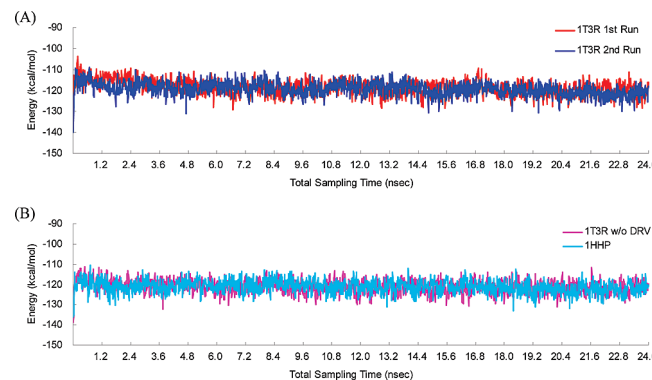


Figure 4. Thermodynamic integration results over total sampling time showing that the calculations are stable. (A) $\Delta G_{\text{complex}}$ from two independent calculations of the coordinates of the DRV–WT crystal structure (1T3R). (B) ΔG_{apo} from two independent starting calculations from different starting structures: the DRV–WT crystal structure (1T3R) with the inhibitor removed is colored magenta, and the apo protease crystal structure (1HHP) is colored cyan.

several studies involving different protein–ligand systems.^{50–53} Such bias did not affect the ranking of binding energies for a given receptor with different ligands or for receptor variants with a specific ligand. Consistent with the results in other systems,⁵¹ the MM-GBSA and MM-PBSA methods provide the same rank order of binding energies (Table 2) although the absolute values were different, for complexes of HIV-1 protease with DRV.

3.1.2. Calculation of Relative Binding Free Energy. For the ACT double mutant V82T–I84V, the relative binding free energy was also calculated by the more rigorous and computationally more intensive thermodynamic integration method. This method has proven to be a powerful tool for studying binding free energy differences in a receptor–ligand system as statistical mechanics is its theoretical framework.^{16,54} As described in the Methods section, thermodynamic integration calculated the binding free energy change from WT–DRV to ACT–DRV. The free energy changes associated with the alchemical pathways ΔG_{apo} and $\Delta G_{\text{complex}}$, which were the sum of 12 weighted $dV/d\lambda$ values (see eq 5, Table S1, Supporting Information), were plotted versus the time for the study of calculation convergence (Figure 4). For thermodynamic integration calculations, their reproducibility and internal consistency were studied by setting up two sets of independent simulations. Comparison of the two calculations of $\Delta G_{\text{complex}}$, which were started from the DRV–WT complex crystal structure coordinates, resulted in using the first 0.5 ns of each of the 12 λ values as the equilibration period and the second 1.5 ns of each of the 12 λ values as the production period. The total time for the equilibration period and production period were 6 and 18 ns, respectively. The two $\Delta G_{\text{complex}}$ values were -119.3 kcal/mol for run 1

Table 2. Difference between the MM-GBSA and MM-PBSA Calculations (kcal/mol)

protease	$\Delta G_{\text{SOLV-GB}}$	$\Delta G_{\text{SOLV-PB}}$	$\Delta G_{\text{CAL-GB}}$	$\Delta G_{\text{CAL-PB}}$	ΔG_{EXP}^a
WT	52.8 ± 0.2	64.4 ± 0.4	-26.7 ± 1.8	-15.1 ± 1.8	-15.2 ± 0.3
FLAP+	53.9 ± 0.2	63.3 ± 0.3	-21.0 ± 1.5	-11.6 ± 1.5	-14.2 ± 0.1
ACT	52.3 ± 0.2	60.2 ± 0.4	-18.4 ± 1.7	-10.5 ± 1.7	-13.6 ± 0.2

^a Experimental binding free energy data were obtained by ITC^{5,66}

Table 3. Thermodynamic Integration Calculation over 12 λ on the Equilibration and Production Periods (kcal/mol)

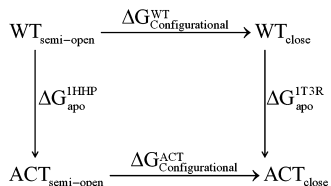
period	$\Delta G_{\text{complex}}$		ΔG_{apo}		$\Delta \Delta G^a$
	1T3R first run	1T3R second run	1HHP	1T3R w/o DRV	
equilibration period ^b	-116.1 ± 0.2	-118.1 ± 0.2	-120.7 ± 0.2	-119.9 ± 0.2	3.2 ± 0.4
production period ^b	-119.3 ± 0.1	-119.9 ± 0.1	-121.3 ± 0.1	-121.5 ± 0.1	1.8 ± 0.2

^a $\Delta \Delta G = \text{Mean}(\Delta G_{\text{complex}} - \Delta G_{\text{apo}})$. ^b Note that the equilibration period is the first 0.5 ns of each of the 12 λ 's, and the production period is the second 1.5 ns of each of the 12 λ 's, of the entire calculation. Total equilibration time is 6 ns, and production time is 18 ns.

Table 4. Relative Binding Free Energy (kcal/mol) of ACT and WT HIV-1 Protease Calculated by Thermodynamic Integration, MM-GBSA, and MM-PBSA Methods vs ITC Data⁵

thermodynamic integration	MM-GBSA	MM-PBSA	ITC
$\Delta \Delta G$	1.8 ± 0.2	8.3 ± 3.5	4.6 ± 3.5

and -119.9 kcal/mol for run 2 (Table 3). The ΔG_{apo} values calculated from the 1HHP and 1T3R crystal structure coordinates were -121.3 and -121.5 kcal/mol, respectively (Table 3). The protease in the 1HHP crystal structure has a flap semiopen conformation. The one in the 1T3R crystal structure has a flap close conformation. The free energy change ($\Delta G_{\text{Configurational}}$) associated with the transition from the semiopen conformations to the closed conformations protease was related to ΔG_{apo} as shown in the thermodynamic cycle below: in which



$$\Delta G_{\text{apo}}^{\text{1HHP}} - \Delta G_{\text{apo}}^{\text{1T3R}} = \Delta G_{\text{Configurational}}^{\text{WT}} - \Delta G_{\text{Configurational}}^{\text{ACT}}$$

The highly similar results of ΔG_{apo} calculated from both 1HHP and 1T3R structures indicated that the WT and the ACT had similar $\Delta G_{\text{Configurational}}$ values between their semiopen and close conformations. The relative binding free energy between DRV-WT and DRV-ACT was 1.8 kcal/mol. This result was a better match with the experimental relative binding free energy of 1.6 kcal/mol than 4.6 and 8.3 kcal/mol, which were calculated from the MM-PBSA and MM-GBSA methods, respectively (Table 4).

3.2. Free-Energy Decomposition Analysis. **3.2.1. Analysis of Contributions from Different Energy Components.** A free energy component analysis was performed to elucidate the mechanism for resistance to DRV of FLAP+ and ACT. The different energy components in the MM-PB/GBSA model (see the Methods section) were shown in Figure 5 and tabulated in the Supporting Information in more detail (Table S2). Both translational entropy ($-T\Delta S_{\text{translational}}$) change and rotational entropy change ($-T\Delta S_{\text{rotational}}$) were close in value in DRV binding for the three protease variants (Supporting Information, Table S2). They represented at least 90% of the change in entropy. The remaining vibration entropy change ($-T\Delta S_{\text{vibrational}}$) was 1.5 kcal/mol for DRV-WT binding, 2.2 kcal/mol for DRV-Flap+, and 0.2 kcal/mol

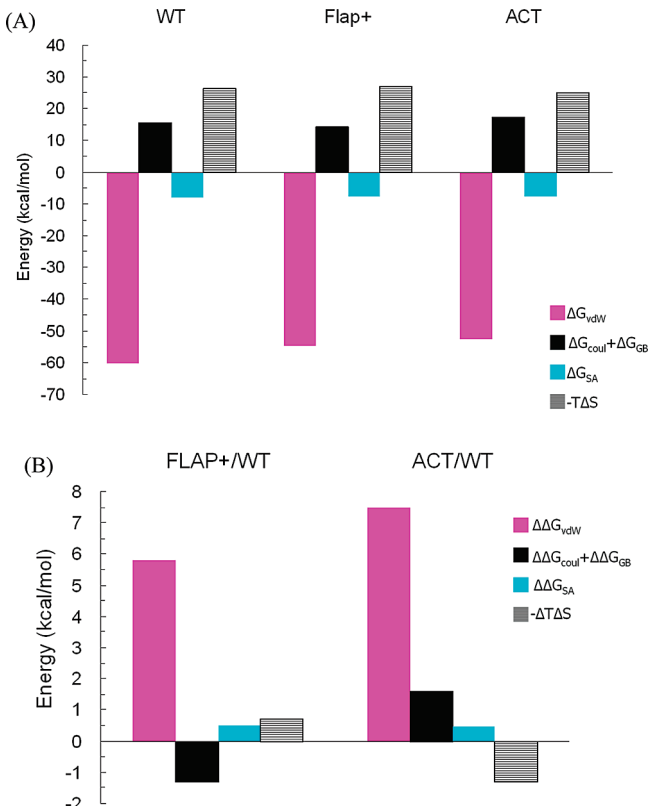


Figure 5. (A) Binding free energy components of DRV-WT, DRV-FLAP+, and DRV-ACT. (B) The loss of binding free energy components with DRV of FLAP+ and ACT compared to the WT protease.

for DRV-ACT. Further free-energy component analysis revealed that the favorable electrostatic interaction energy term (ΔG_{ELE}) from the molecular mechanical energy (ΔG_{MM}) had been canceled by the unfavorable polar solvation energy (ΔG_{GB}) penalty. This result was in agreement with other MM-PB/GBSA studies.^{24,55-58} The total electrostatic interaction energy ($\Delta G_{\text{ELE}} + \Delta G_{\text{GB}}$) for DRV-WT was 15.4 kcal/mol, for DRV-FLAP+ was 14.1 kcal/mol, and for DRV-ACT was 17.0 kcal/mol. The vdW interaction energy was -60.3 kcal/mol for DRV-WT, -54.5 kcal/mol for DRV-FLAP+, and -52.8 kcal/mol for DRV-ACT. The vdW interactions had the largest contribution to protease-inhibitor binding (Figure 5A) and sustained the largest energy loss in both the FLAP+ and ACT drug-resistant mutants (Figure 5B).

3.2.2. Free Energy Projected to Each Residue of HIV-1 Protease. In order to gain extra insight into the mechanisms of protease-inhibitor binding and drug resistance, the binding free energy calculated from the MM-GBSA method had been broken down to individual protease residues. The

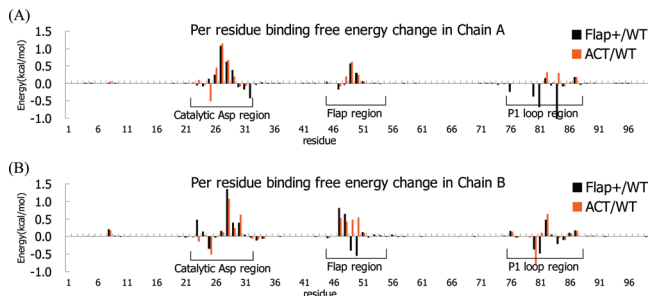


Figure 6. Decomposition of energy from MM-GBSA per residue of HIV-1 protease. (A) Energy difference between wild-type protease and FLAP+ variant. (B) Energy difference between wild-type protease and ACT variant.

energy difference was investigated between the WT–DRV complex and the two drug-resistant mutant protease–DRV complexes for each residue (Figure 6). The residues with energy changes were mainly located in three areas (Supporting Information, Figure S3), the catalytic region (residues 22 to 33), the flap region (residues 45 to 55), and the P1 loop region (residues 79 to 87) on both monomers of the protease. These energy changes varied asymmetrically in the two protease monomers. Many residues (27, 28, 50, 87, 8', 28', 29', 47', and 76') structurally adjacent to DRV other than those that mutate (10, 48, 54, and 82 for FLAP+; 82 and 84 for ACT) responded to the mutations (Figure 6) as had been previously observed.^{14,28} The sites of mutation not only impacted their own binding free energy interactions with inhibitors but also influenced the interaction of other residues with the inhibitor by inducing alterations in the geometry of the binding site.

Favorable electrostatic interactions opposed by the polar solvation energy penalty also apply to individual residues. A change in electrostatic energy ($\Delta\Delta G_{ELE}$) of any residue was always associated with an equal but opposite compensation in solvation energy ($\Delta\Delta G_{GB}$) of very similar amplitude but in a different direction. The correlation coefficient for the $\Delta\Delta G_{ELE}$ and $\Delta\Delta G_{GB}$ of FLAP+ was -0.97 and for the ACT was -0.95 (Figure 7A for FLAP+, Figure 7B for ACT). This high correlation of $\Delta\Delta G_{ELE}$ and $\Delta\Delta G_{GB}$ made the change of vdW energy the largest factor in the loss of binding free energy between DRV and FLAP+/ACT. The residues in the catalytic, flap, and P1 loop regions also had the largest change in vdW interaction energy (Figure 8). To highlight those residues with a significant difference between the WT and the two drug-resistant mutants, a cutoff of 0.1 kcal/mol of vdW energy change was used. The residues in FLAP+ and ACT with a loss of vdW energy greater than the cutoff were plotted in Figure 8C. In chain A, these residues included 26, 27, 28, 47, 49, and 50; in chain B, these residues were 8', 25', 27'-31', 47'-49', 51', 52', 54', 76', 82', and 86' (Supporting Information Figure S3D). The loss in vdW interaction energy of chain B was significantly larger than that of chain A.

3.2.3. vdW Energy Contribution from Each DRV Atom. To explore the mechanism of the loss in binding free energy between DRV and the drug-resistant mutants, the vdW energy contributions were calculated for each DRV atom

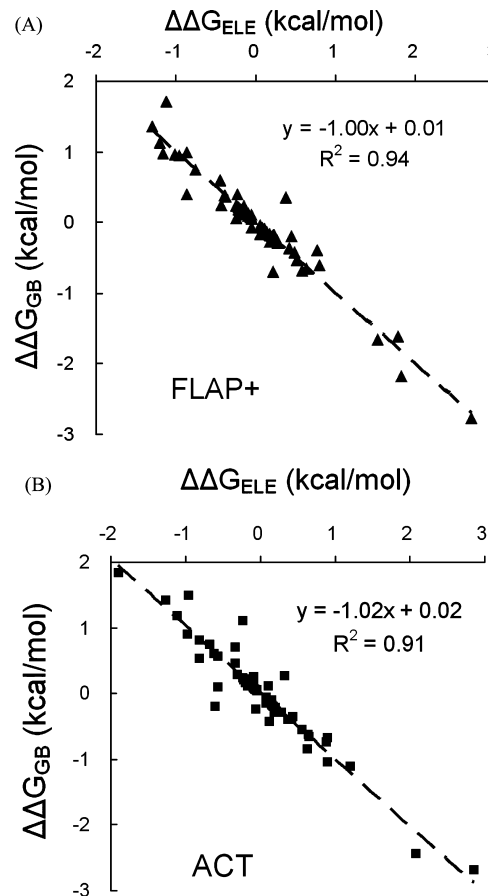


Figure 7. Correlation between $\Delta\Delta G_{ELE}$ and $\Delta\Delta G_{GB}$ of each residue. (A) Energy difference between FLAP+ and WT. (B) Energy difference between ACT and WT.

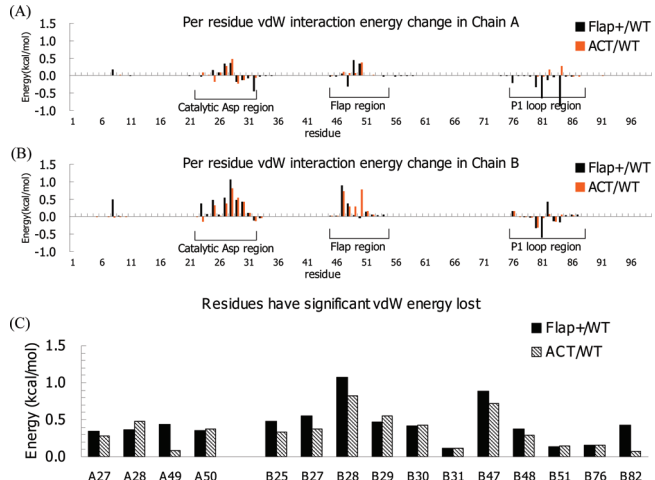


Figure 8. (A) vDW energy loss between FLAP+ and WT protease. (B) vDW energy loss between ACT and WT protease. (C) Residues with a vDW energy loss larger than 0.1 kcal/mol.

and compared between complexes with the WT and FLAP+ and ACT mutant proteases. DRV had 75 atoms, of which 37 were hydrogen atoms with very limited contribution to the vDW interaction energy. Thus, data were presented for only the 38 heavy atoms in DRV (Figure 9A). Structurally, DRV could be considered formed by four major moieties:

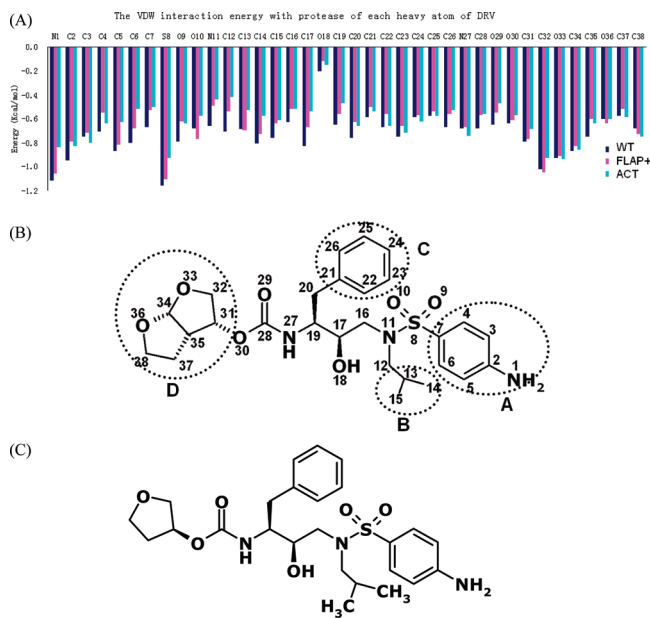


Figure 9. (A) vdW interaction energy of each non-hydrogen atom of DRV with protease. The energy of DRV–WT is colored dark blue, the energy of DRV–FLAP+ is colored magenta, and the energy of DRV–ACT is colored cyan. (B) The definition of four moieties of DRV. (C) The chemical structure of APV.

(A) the 4-amino phenyl group, (B) the isopropyl group, (C) the benzyl ring, and (D) *bis*-tetrahydrofuranylurethane (THF; Figure 9B). To compare the energy change between these 4 moieties, we defined DV (loss of vdW interaction energy ratio) as

$$DV = \frac{\sum_i (E_i^{\text{Flap}+} - E_i^{\text{WT}}) + \sum_i (E_i^{\text{ACT}} - E_i^{\text{WT}})}{2 \times \sum_i E_i^{\text{WT}}} \times 100\%$$

where i is the atom within a specific moiety. The *bis*-THF moiety and the benzyl ring have relatively low DVs of 3.1% and 8.5%, respectively. The 4-amino phenyl and isobutyl groups have significantly higher DVs of 17.0% and 19.2%, respectively (Table 5).

The major difference between DRV and a previous generation protease inhibitor, amprenavir (APV; Figure 9C), is that DRV has a second tetrahydrofuran ring, which is part of its *bis*-THF moiety. Nonetheless, DRV has been shown by ITC experiments⁵ to bind more tightly than APV with the protease, with a 2.6 kcal/mol larger binding affinity. In the DRV–WT protease structure (1T3R), the *bis*-THF moiety is surrounded by the protease chain A residues Ala28, Asp29, Asp30, Ile47, Gly48, and Gly49, which form a cluster of vdW contacts (Figure 10A and B). This packing can be also observed from the crystal structures of the DRV–FLAP+ and DRV–ACT complexes.⁵ Examination of the MD

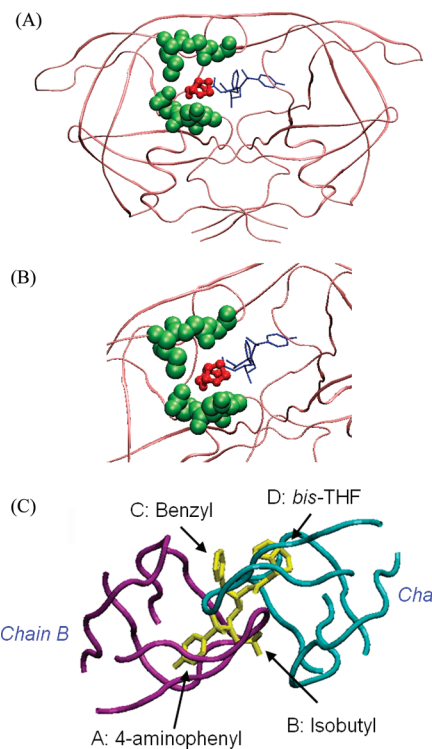


Figure 10. (A and B) Cluster of vdW contacts formed by the *bis*-THF group and the protease residues Ala28, Asp29, Asp30, Ile47, Gly48, and Gly49 of chain A. The atoms of the above residues are displayed and colored green. The atoms of the *bis*-THF group are colored red, while the rest of DRV is colored blue. (C) Relative position of DRV's four moieties (colored yellow) to chain A (colored cyan) and chain B (colored purple) of protease.

simulation structures of DRV in complex with the WT, FLAP+, and ACT proteases showed that these residues and the *bis*-THF moiety maintained a relatively stable structure compared to other parts of the inhibitor. This stability led to the small ratio of the *bis*-THF group's vdW energy loss (Table 5).

Similar to the *bis*-THF group, the benzyl ring maintained its vdW interactions with protease residues in chain A (Figure 10C) in most conformations sampled by the MD simulations. This stability in DRV interactions with chain A explained the asymmetric vdW energy losses of the protease's two chains. Chain B was shown by free-energy decomposition of protease residues to have more residues with significant energy loss than chain A (Figure 8C). Unlike the *bis*-THF group and the benzyl ring, whose vdW interactions were only slightly influenced by the drug-resistant mutations, the 4-amino phenyl and isobutyl groups of DRV in complex with FLAP+ and ACT lost approximately 20% of the vdW interaction energy. A comparison of the MD simulation structure of DRV–WT with those of the two drug-resistant mutants showed that the 4-amino phenyl and isobutyl groups of DRV in the DRV–FLAP+ and DRV–ACT complexes

Table 5. Loss of van der Waals' Interaction Energy (DV) for Different DRV Moieties

	4-amino phenyl group	isobutyl group	benzyl ring	<i>bis</i> - tetrahydrofuranyl
DV (%) number of heavy atoms	17 7	19 4	9 7	3 8

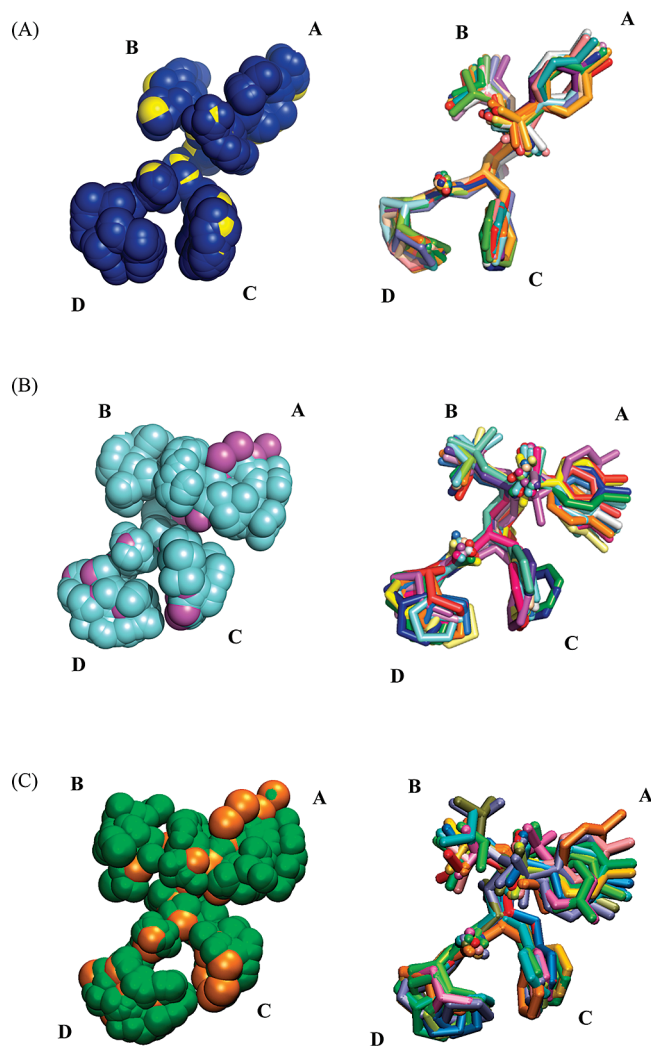


Figure 11. (A) Conformational space of DRV sampled in DRV–WT complex simulations. Left: DRV ensemble is shown with atoms' vdW radii. The original conformation as in the crystal structure is colored yellow. The sampled conformations ensemble from MD simulation is colored blue. Right: 20 snapshots of DRV conformations taken every 1 ns from MD simulations. (B) Conformational space of DRV sampled in DRV–FLAP+ complex simulations. Left: DRV ensemble is shown with atoms' vdW radii. The original conformation as in the crystal structure is colored purple. The sampled conformations ensemble from MD simulation is colored cyan. Right: 20 snapshots of DRV conformations taken every 1 ns from MD simulations. (C) Conformational space of DRV sampled in DRV–ACT complex simulations. Left: DRV ensemble is shown with atoms' vdW radii. The original conformation as in the crystal structure is colored orange. The sampled conformations ensemble from MD simulation is colored green. Right: 20 snapshots of DRV conformations taken every 1 ns from MD simulations.

undergo significant geometry changes (Figure 11A and B) that led to these groups losing their vdW contacts with the drug-resistant proteases.

The free-energy decomposition by residue showed that the mutations had induced changes in the shape of the binding pocket as evidenced by the predominant changes occurring in the vdW interactions energy. Overall, there was a decrease in the vdW interaction energy between the protease and

DRV, mostly on the 4-amino phenyl side, as the volume of the binding pocket was effectively enlarged as the mutations within the active site were to smaller residues (V82A in Flap+ and I84V in ACT). This expansion of the active site permits, as we had observed, other residues to interact to varying degrees with the inhibitor; in this way, the FLAP+ and ACT mutant proteases could develop drug resistance.

4. Conclusion and Discussion

With the appearance of drug-resistant HIV-1 protease variants becoming one of the major challenges to AIDS therapy, understanding the mechanism of drug resistance is critical. This goal is best addressed by cross-analyzing the data on protease mutants from different experimental methods such as crystallography and isothermal titration calorimetry.^{59–62} Comparing the crystal structure of APV bound to wild-type protease and a drug-resistant protease variant, King et al.⁵ found that the mutation I84V has decreased the vdW interaction between APV and the drug-resistant variant, which might account for the loss of binding affinity between APV and the drug-resistant variant. By analyzing the ITC experiments results, Luque et al.⁵⁹ suggested that the drug-resistant mutations change the shape of the active site. The very flexible substrates are less susceptible to the change than the synthetic inhibitors,⁵⁹ which might enable the drug-resistant protease variant to still recognize the substrate while having less binding affinity with the synthetic inhibitors. Comparing the trajectories from MD simulations on the wild-type protease and the V82F/I84V protease variant, Perryman et al.⁶³ suggested that the mutations changing the equilibrium between the flap-semiopen and closed conformations could be one aspect of the protease drug-resistant mechanism. More details about inhibitor–protease binding can be provided by free energy calculations, which start from structural coordinates and yield thermodynamic data. In this study, we performed MM-PB/GBSA calculations and free-energy component analysis of DRV–WT, DRV–FLAP+ (L10I, G48V, I54V, V82A), and DRV–ACT (V82T, I84V). By running three independent 20 ns simulations for each of these systems, we not only identified the convergence and consistency of our calculations but also predicted the order of binding energies in agreement with ITC data. As described in the Methods section, the calculations of solvation energy and molecular mechanic energy were based on 1000 frames with a 20 ps interval. The more time-consuming entropy calculation was based on 100 frames with a 200 ps interval. In order to examine the statistical significance of the binding free energy of protease with DRV, we calculated the entropy for each frame that was used to calculate the solvation energy and the molecular mechanic energy. The difference of calculated entropy using 100 frames and 1000 frames was tabulated in the Supporting Information (Table S3). *t* tests were performed to evaluate the significance of the difference of $\Delta G_{\text{MM-PBSA}}$ and $\Delta G_{\text{MM-GBSA}}$ between WT, Flap+, and ACT. The *p* values were all less than 0.01, which indicated significant differences.

Moreover, the relative binding free energy between DRV–WT and DRV–ACT using MM-PB/GBSA and thermodynamic integration (TI) methods was calculated. The

accuracy of these result had the rank order TI > MM-PBSA > MM-GBSA, which is the same order of the computational times required for these methods. The TI method is more suitable for comparing the energy difference between two similar systems. In the case of the ACT (V82T, I84V) mutant here, the TI method not only gave the more accurate predicted energy than the MM-PB/GBSA method but also had better reproducibility and faster convergence (Figure 3, Figure 4).

The results of free energy components analysis showed that the vdW interaction energy was dominant in the total binding free energy change. The contribution from charged interactions was minor compared to vdW interactions due to the cancellation of electrostatic interactions energy and the polar desolvation energy. Interestingly, a previous free energy component analysis showed that, compared to the total predicted binding free energy, the predicted contribution from electrostatic interaction had a higher correlation with the experimental binding free energy.⁶⁴ Recently, a similar analysis from the same group on interactions between HIV protease and inhibitors concluded that the total theoretical binding energy was in agreement with the experimental data, although the free energy component from only the charged interactions was also correlated well with experimental binding free energy.⁶⁵ This difference might have resulted from the different environments of the two systems.⁶⁵ The former calculation was on the large solvated protein surface, while the latter calculation on HIV protease was on a relatively small and buried binding pocket. The free-energy decomposition analysis on protease residues indicated that mutations in the protease induced conformational changes in its active site. The bis-THF group and benzyl ring of DRV sustained their vdW interactions with the drug-resistant protease variants and contribute most to the inhibitor–protease binding, while DRV's 4-amino phenyl and isobutyl groups were susceptible to changes in the protease's binding pocket and adopted conformations that lose vdW interaction with drug-resistant variants (Table 5).

These findings suggested that the design of new protease inhibitors based on the DRV scaffold should consider reoptimizing 4-aminophenyl and isopropyl groups since these parts of DRV did not maintain their interactions with drug resistant protease variants as much as the bis-THF group. Such new inhibitors would likely bind more tightly to HIV protease and may be less susceptible to drug resistance.

Abbreviations

Bis-THF, bis-tetrahydrofuryl; ITC, isothermal titration calorimetry; TI, thermodynamic integration; MM-PBSA, molecular mechanics–Poisson–Boltzmann surface area; GB, generalized Born; DRV, Darunavir; ACT, HIV-1 protease variant V82T, I84 V; FLAP+, HIV-1 protease variant L10I, G48V, I54 V, V82A; vdW, van der Waals; MD, molecular dynamics; ns, nanosecond; ps, picosecond; fs, femtosecond.

Acknowledgment. We acknowledge Nancy King, Moses Prabu, Ellen Nalivaika, and Madhavi Nalam in the acquisition of the experimental data. We also acknowledge Claire Baldwin for the preparation of the manuscript. This

research was supported by the National Institutes of Health (NIH), grant P01-GM66524. Calculations were performed on a computer cluster purchased with NIH 1S10440166892993.

Supporting Information Available: Figures of MM-GBSA calculated results of DRV-Flap+, DRV-ACT binding free energy with respect to the time; plots of the rmsd of C α atoms of protease with respect to their corresponding crystal structures over time; Tables S1 and S2. This material is available free of charge via the Internet at <http://pubs.acs.org/>.

References

- (1) Debouck, C. *AIDS Res. Hum. Retroviruses* **1992**, *8*, 153.
- (2) Wlodawer, A.; Erickson, J. W. *Annu. Rev. Biochem.* **1993**, *62*, 543.
- (3) Wood, E.; Hogg, R. S.; Yip, B.; Moore, D.; Harrigan, P. R.; Montaner, J. S. *HIV Med.* **2007**, *8*, 80.
- (4) Schinazi, R. F.; Larder, B. A.; Mellors, J. W. *Int. Antiviral News* **1997**, *5*, 129.
- (5) King, N. M.; Prabu-Jeyabalan, M.; Nalivaika, E. A.; Wigerinck, P.; de Bethune, M. P.; Schiffer, C. A. *J. Virol.* **2004**, *78*, 12012.
- (6) Todd, M. J.; Luque, I.; Velazquez-Campoy, A.; Freire, E. *Biochemistry* **2000**, *39*, 11876.
- (7) King, N. M.; Melnick, L.; Prabu-Jeyabalan, M.; Nalivaika, E. A.; Yang, S. S.; Gao, Y.; Nie, X.; Zepp, C.; Heefner, D. L.; Schiffer, C. A. *Protein Sci.* **2002**, *11*, 418.
- (8) Prabu-Jeyabalan, M.; Nalivaika, E. A.; King, N. M.; Schiffer, C. A. *J. Virol.* **2003**, *77*, 1306.
- (9) Talhout, R.; Villa, A.; Mark, A. E.; Engberts, J. B. *J. Am. Chem. Soc.* **2003**, *125*, 10570.
- (10) Huang, N.; Jacobson, M. P. *Curr. Opin. Drug Discovery Dev.* **2007**, *10*, 325.
- (11) Jorgensen, W. L. *Science* **2004**, *303*, 1813.
- (12) Bash, P. A.; Singh, U. C.; Brown, F. K.; Langridge, R.; Kollman, P. A. *Science* **1987**, *235*, 574.
- (13) Wang, W.; Kollman, P. A. *Proc. Natl. Acad. Sci. U. S. A.* **2001**, *98*, 14937.
- (14) Wittayanarakul, K.; Aruksakunwong, O.; Sompornpisut, P.; Sanghiran-Lee, V.; Parasuk, V.; Pinitglang, S.; Hannongbua, S. *J. Chem. Inf. Model.* **2005**, *45*, 300.
- (15) Adcock, S. A.; McCammon, J. A. *Chem. Rev.* **2006**, *106*, 1589.
- (16) Gao, J.; Kuczera, K.; Tidor, B.; Karplus, M. *Science* **1989**, *244*, 1069.
- (17) Zwanzig, R. W. *J. Chem. Phys.* **1954**, *22*, 1420.
- (18) Michelin, O.; Karplus, M. *J. Mol. Biol.* **2002**, *324*, 547.
- (19) Archontis, G.; Simonson, T.; Moras, D.; Karplus, M. *J. Mol. Biol.* **1998**, *275*, 823.
- (20) Singh, U. C.; Benkovic, S. J. *Proc. Natl. Acad. Sci. U. S. A.* **1988**, *85*, 9519.
- (21) Lawrence, M.; Baron, R.; McCammon, J. A. *J. Chem. Theory Comput.* **2009**, *5*, 1106.
- (22) Massova, I.; Kollman, P. A. *Perspect. Drug Discovery Des.* **1999**, *18*, 113.

- (23) Xu, Y.; Wang, R. *Proteins* **2006**, *64*, 1058.
- (24) Gohlke, H.; Kiel, C.; Case, D. A. *J. Mol. Biol.* **2003**, *330*, 891.
- (25) Archontis, G.; Simonson, T.; Karplus, M. *J. Mol. Biol.* **2001**, *306*, 307.
- (26) Swanson, J. M.; Henchman, R. H.; McCammon, J. A. *Biophys. J.* **2004**, *86*, 67.
- (27) Hendsch, Z. S.; Tidor, B. *Protein Sci.* **1999**, *8*, 1381.
- (28) Hou, T.; Yu, R. *J. Med. Chem.* **2007**, *50*, 1177.
- (29) Surleraux, D. L.; Tahri, A.; Verschueren, W. G.; Pille, G. M.; de Kock, H. A.; Jonckers, T. H.; Peeters, A.; De Meyer, S.; Azijn, H.; Pauwels, R.; de Bethune, M. P.; King, N. M.; Prabu-Jeyabalan, M.; Schiffer, C. A.; Wigerinck, P. B. *J. Med. Chem.* **2005**, *48*, 1813.
- (30) Surleraux, D. L.; de Kock, H. A.; Verschueren, W. G.; Pille, G. M.; Maes, L. J.; Peeters, A.; Vendeville, S.; De Meyer, S.; Azijn, H.; Pauwels, R.; de Bethune, M. P.; King, N. M.; Prabu-Jeyabalan, M.; Schiffer, C. A.; Wigerinck, P. B. *J. Med. Chem.* **2005**, *48*, 1965.
- (31) Case, D. A.; Cheatham, T. E., III; Darden, T.; Gohlke, H.; Luo, R.; Merz, K. M., Jr.; Onufriev, A.; Simmerling, C.; Wang, B.; Woods, R. J. *J. Comput. Chem.* **2005**, *26*, 1668.
- (32) Duan, Y.; Wu, C.; Chowdhury, S.; Lee, M. C.; Xiong, G.; Zhang, W.; Yang, R.; Cieplak, P.; Luo, R.; Lee, T.; Caldwell, J.; Wang, J.; Kollman, P. A. *J. Comput. Chem.* **2003**, *24*, 1999.
- (33) Wang, J.; Wolf, R. M.; Caldwell, J. W.; Kollman, P. A.; Case, D. A. *J. Comput. Chem.* **2004**, *25*, 1157.
- (34) Frisch, M. J.; Trucks, G. W.; Schlegel, H. B.; Scuseria, G. E.; Robb, M. A.; Cheeseman, J. R.; Montgomery, J. A., Jr.; Vreven, T.; Kudin, K. N.; Burant, J. C.; Millam, J. M.; Iyengar, S. S.; Tomasi, J.; Barone, V.; Mennucci, B.; Cossi, M.; Scalmani, G.; Rega, N.; Petersson, G. A.; Nakatsuji, H.; Hada, M.; Ehara, M.; Toyota, K.; Fukuda, R.; Hasegawa, J.; Ishida, M.; Nakajima, T.; Honda, Y.; Kitao, O.; Nakai, H.; Klene, M.; Li, X.; Knox, J. E.; Hratchian, H. P.; Cross, J. B.; Adamo, C.; Jaramillo, J.; Gomperts, R.; Stratmann, R. E.; Yazayev, O.; Austin, A. J.; Cammi, R.; Pomelli, C.; Ochterski, J. W.; Ayala, P. Y.; Morokuma, K.; Voth, G. A.; Salvador, P.; Dannenberg, J. J.; Zakrzewski, V. G.; Dapprich, S.; Daniels, A. D.; Strain, M. C.; Farkas, O.; Malick, D. K.; Rabuck, A. D.; Raghavachari, K.; Foresman, J. B.; Ortiz, J. V.; Cui, Q.; Baboul, A. G.; Clifford, S.; Cioslowski, J.; Stefanov, B. B.; Liu, G.; Liashenko, A.; Piskorz, P.; Komaromi, I.; Martin, R. L.; Fox, D. J.; Keith, T.; Al-Laham, M. A.; Peng, C. Y.; Nanayakkara, A.; Challacombe, M.; Gill, P. M. W.; Johnson, B.; Chen, W.; Wong, M. W.; Gonzalez, C.; Pople, J. A. *Gaussian 03*, Revision B.05; Gaussian, Inc.: Pittsburgh, PA, 2003.
- (35) Bayly, C. I. C., P.; Cornell, W. D.; Kollman, P. A. *J. Phys. Chem.* **1993**, *97*, 10269.
- (36) Ryckaert, J.-P.; Ciccotti, G.; Berendsen, H. J. C. *J. Comput. Phys.* **1977**, *23*, 327.
- (37) Onufriev, A.; Case, D. A.; Bashford, D. *J. Comput. Chem.* **2002**, *23*, 1297.
- (38) Onufriev, A.; Bashford, D.; Case, D. A. *Proteins* **2004**, *55*, 383.
- (39) Luo, R.; David, L.; Gilson, M. K. *J. Comput. Chem.* **2002**, *23*, 1244.
- (40) Sitkoff, D.; Sharp, K. A.; Honig, B. *J. Phys. Chem.* **1994**, *98*, 1978.
- (41) Gilson, M. K.; Given, J. A.; Bush, B. L.; McCammon, J. A. *Biophys. J.* **1997**, *72*, 1047.
- (42) Kollman, P. A. *Chem. Rev.* **1993**, *93*, 2395.
- (43) Radmer, R. J.; Kollman, P. A. *J. Comput.-Aided Mol. Des.* **1998**, *12*, 215.
- (44) Lau, F. T.; Karplus, M. *J. Mol. Biol.* **1994**, *236*, 1049.
- (45) Blondel, A. *J. Comput. Chem.* **2004**, *25*, 985.
- (46) Wong, C. F.; McCammon, J. A. *J. Am. Chem. Soc.* **1986**, *108*, 3830.
- (47) Case, D. A.; Cheatham, T. E., III; Darden, T.; Gohlke, H.; Luo, R.; Merz, K. M., Jr.; Onufriev, A.; Simmerling, C.; Wang, B.; Woods, R. J. *J. Comput. Chem.* **2005**, *26*, 1668.
- (48) Lee, T.; Kollman, P. A. *J. Am. Chem. Soc.* **2000**, *122*, 4385.
- (49) Bishop, M.; Frinks, S. *J. Phys. Chem.* **1987**, *87*, 3675.
- (50) Bea, I.; Gotsev, M. G.; Ivanov, P. M.; Jaime, C.; Kollman, P. A. *J. Org. Chem.* **2006**, *71*, 2056.
- (51) Wittayanarakul, K.; Hannongbua, S.; Feig, M. *J. Comput. Chem.* **2008**, *29*, 673.
- (52) Gohlke, H.; Case, D. A. *J. Comput. Chem.* **2004**, *25*, 238.
- (53) Ferrara, P.; Gohlke, H.; Price, D. J.; Klebe, G.; Brooks, C. L. *J. Med. Chem.* **2004**, *47*, 3032.
- (54) Lee, T.; Kollman, P. A. *J. Am. Chem. Soc.* **2000**, *122*, 4385.
- (55) Stoica, I.; Sadiq, S. K.; Coveney, P. V. *J. Am. Chem. Soc.* **2008**, *130*, 2639.
- (56) Massova, I.; Kollman, P. A. *J. Am. Chem. Soc.* **1999**, *11*, 8133.
- (57) Wang, W.; Kollman, P. A. *J. Mol. Biol.* **2000**, *303*, 567.
- (58) Huo, S.; Massova, I.; Kollman, P. A. *J. Comput. Chem.* **2002**, *23*, 15.
- (59) Luque, I.; Todd, M. J.; Gomez, J.; Semo, N.; Freire, E. *Biochemistry* **1998**, *37*, 5791.
- (60) Todd, M. J.; Luque, I.; Velazquez-Campoy, A.; Freire, E. *Biochemistry* **2000**, *39*, 11876.
- (61) Velazquez-Campoy, A.; Kiso, Y.; Freire, E. *Arch. Biochem. Biophys.* **2001**, *390*, 169.
- (62) Ohtaka, H.; Velazquez-Campoy, A.; Xie, D.; Freire, E. *Protein Sci.* **2002**, *11*, 1908.
- (63) Perryman, A. L.; Lin, J. H.; McCammon, J. A. *Protein Sci.* **2004**, *13*, 1108.
- (64) Lippow, S. M.; Wittrup, K. D.; Tidor, B. *Nat. Biotechnol.* **2007**, *25*, 1171.
- (65) Huggins, D. J.; Altman, M. D.; Tidor, B. *Proteins* **2009**, *75*, 168.
- (66) King, N. M.; Prabu-Jeyabalan, M.; Bandaranayake, R. M.; Nalam, M. N.; Ozen, A.; Haliloglu, T.; Schiffer, C. In preparation 2009.